Wide gap Chern Mott insulating phases achieved by design

Hongli Guo[1,2], Shruba Gangopadhyay[3], Okan Köksal[4],

Rossitza Pentcheva[4], and Warren E. Pickett[5,*]

[1]*ICQD/Hefei National Laboratory for Physical Sciences at Microscale,*

and Key Laboratory of Strongly-Coupled Quantum Matter Physics,

Chinese Academy of Sciences, and Department of Physics,

University of Science and Technology of China, Hefei, Anhui 230026, China

[2]*Synergetic Innovation Center of Quantum Information & Quantum Physics,*

University of Science and Technology of China, Hefei, Anhui 230026, China

[3]*Department of Chemistry, University of California Davis, Davis, California 95616, USA*

[4]*2Department of Physics and Center for Nanointegration Duisburg-Essen (CENIDE),*

University of Duisburg-Essen, 47057 Duisburg, Germany and

[5]*Department of Physics, University of California Davis, Davis, California 95616, USA*

(Dated: July 27, 2016)

Running title: **Wide gap Chern phases by design**

Corresponding author:

Warren E. Pickett **wepickett@ucdavis.edu**

Department of Physics

University of California Davis

Davis CA 95616

ABSTRACT

Quantum anomalous Hall (QAH) insulators, which display robust surface charge and spin currents categorized in terms of a bulk topological invariant known as the Chern number,[1] provide the quantum Hall effect without an applied magnetic field. Chern insulators are attracting interest both as a novel electronic phase and for their novel and potentially useful surface properties. Honeycomb lattice systems such as we discuss here, occupied by heavy transition-metal ions, have been proposed as Chern insulators, but finding a concrete example has been limited due to an assortment of broken symmetry phases that thwart the topological character. Building on accumulated knowledge of the behavior of the $3d$ series, we tune spin-orbit and interaction strength together with strain to design two Chern insulator systems with bandgaps up to 130 meV and Chern numbers $\mathcal{C} = -1$ and $\mathcal{C} = 2$. We find, in this system, that a trade-off between larger spin-orbit coupling and strong interactions leads to a larger gap, whereas the strongest SOC produces a larger magnitude of the Hall conductivity. Symmetry lowering in the course of structural relaxation hampers obtaining QAH character, as pointed out previously; there is only mild symmetry breaking of the bilayer in the robust Chern phases. Recent growth of insulating, magnetic phases in closely related materials with this orientation supports the likelihood that synthesis and exploitation will follow.

I. INTRODUCTION

The honeycomb lattice,[2] particularly in conjunction with its Dirac points and two-valley nature in graphene,[3] has provided the basic platform for a great number of explorations into new phases of matter and new phenomena. Yet the single band, uncorrelated case of graphene is only the simplest level of what can be realized on honeycomb lattices. The recognition that a perovskite (111) bilayer of $LaXO_3$ encased in $LaAlO_3$ (we use the notation 2LXO for an X bilayer, X=transition metal [TM]) provides a honeycomb lattice that led to a call for engineering (*i.e.* design) of a Chern insulator in such systems.[4, 5] The origin of the buckled honeycomb lattice is depicted in Fig. 1. A number of model[6–9] and material-

specific studies[10–16] have probed the possibilities that such systems may offer. The advent of (111)-oriented growth of oxides[17–25] provides a new platform for design of new materials, and especially Chern insulators.

The degree of generalization from graphene is huge. Graphene has a hopping amplitude, or equivalently a velocity, that sets the energy scale, and a two-valley degree of freedom. 2LXO, on the other hand, provides a multi-orbital system with a number of additional degrees of freedom: intraatomic Coulomb repulsion U and Hund's rule spin interaction J_H, cubic crystal field splitting Δ_{cf}, trigonal crystal field splitting δ_{cf}, spin-orbit coupling (SOC) strength ξ, orbital-dependent interatomic hopping amplitudes, and band filling n_d. Altogether, these couple to the lattice to provide two more scales, the Jahn-Teller (λ_{JT}) and breathing (λ_{br}) distortion strengths. This list includes more than ten parameters, and the treatment of them from a model Hamiltonian viewpoint, even within mean field, is formidable. Some of these energy scales have been included in model studies,[9] but the coupling to lattice that we find to be a determining factor is too intricate for model Hamiltonian studies. Interplay of U with large SOC fulfills the requirements of proposed Chern Mott insulators with bandgaps an order of magnitude larger than those studied so far.

An efficient design strategy must seek to identify promising candidates. The density functional theory (DFT) approach is able to treat all the complexities mentioned above straightforwardly as a part of the electronic structure problem, including other factors such as Madelung potential effects. Also, requiring the choice of atoms from certain classes in the periodic table reduces the scope of the design process from a continuous ∼10 dimensional space to a Diophantine set, and presents clear opportunities to experimentalists. For specific realizations (here, atom X) the many energy scales are known or determined self-consistently. DFT+U treatment requires examination of a few types of likely order parameters (charge, spin, orbital, structural), but the possibilities are also constrained by the vast accumulated knowledge of how TM ions behave in oxides, so the computational complexity becomes manageable. Dynamical correlations may need to be incorporated separately, but they are unrealistic without detailed input from DFT on the symmetry-broken ground states.[12]

Two of the current authors have carried out a systematic study of the entire sequence of $3d$ TM ions on this buckled honeycomb lattice.[14] In three cases X=Ti, Mn, and Co, a Chern insulating phase was obtained as U was varied and the structure relaxed,[14] but the combination of relatively large $U \sim 5$ eV and accompanying distortion resulted in trivial Mott

insulating ground states. However, that study provided the necessary guidance for design of Chern phases in this class of nanostructures. The required properties include: reducing Coulomb repulsion U giving less tendency toward structural distortion, while retaining the Mott gap; increase SOC strength ξ to promote band entanglement and also enhance the gap; use the ability to tune behavior by strain. We have applied these guidelines to explore $4d$ and $5d$ 2LXO bilayers, finding Chern insulating ground states for both the osmate and the ruthenate members, with gaps up to 30 times larger than previously designed TMO Chern insulators: ultrathin VO_2[26, 27] and CrO_2[28] layers with calculated gaps of 2 meV and 4 meV respectively.

Interest in $5d$ ions on the honeycomb lattice has focused primarily on the Ir ion,[10, 11, 18, 21] which is not a part of this study. We consider specifically the $3d \rightarrow 4d \rightarrow 5d$ sequence of ions; for d^4: Mn, Tc, Re; for d^5: Fe, Ru, Os. With the considerable changes versus size and chemistry of the TM ion, we have found that the favorable cases shift from one column (d^4) to the next (d^5) in the periodic table. 2LOsO, with smallest U and largest SOC, might be the first guess as the most promising candidate. Unexpectedly, we find that the intermediate $4d$ Ru ion provides the most promising candidate of Chern insulator in this structural class.

For $SrIrO_3$ iridates (also d^5), there are competing indications whether the bilayer perovskite platform will be both ferromagnetic (FM) and insulating as required for a Chern insulator, or rather will assume some less desirable configuration.[10, 17, 22] It is highly encouraging that (111)-grown $SrIrO_3$ and (Ca,Sr)IrO_3 have been synthesized, with the former found to be magnetic and insulating.[18, 22] We provide below detailed predictions that, once all effects are accounted for, 2LRuO and 2LOsO buckled honeycomb lattices will be Chern insulators with substantial gaps.

II. RESULTS

DFT+U calculations (see the Methods section and Ref. [14]) have been performed for the $4d$ candidates X=Tc and Ru, and the $5d$ examples X=Re and Os, in the Mn d^4 and Fe d^5 columns respectively. Two in-plane lattice constants are considered, $LaAlO_3$ (LAO) denoted a_{LAO} (3.79Å) and $LaNiO_3$ (LNO) denoted a_{LNO} (3.86Å), differing by only 1.8%, still this amount of strain is found to tip the balance between Chern and trivial ground states.

Previous DFT studies on Os based oxide compounds adopted values of U in the range 0.8-3 eV. [25, 29–31] We use U_{Os}=1 eV, U_{Ru}=3 eV and find that results are not very sensitive to reasonable variations around these values. The isovalent $3d$ Fe requires $U_{Fe}\approx$5 eV, leading to a high spin state unlike the low spin $S = \frac{1}{2}$ state we obtain for Ru and Os. Whereas the high spin ion is spherically symmetric (hence not subject to Jahn-Teller distortion), the low spin state will be more susceptible to distortion.

Substantial differences due to transition metal size and chemistry appear immediately. In the $3d$ series, 2LMnO provided the most instructive example, by transforming from a Chern insulator phase to a trivial insulator result, during which a JT distortion closes the Chern gap and then reopens a trivial gap. The isovalent partners X=Tc and Re can be dismissed. Tc^{3+} is FM but with considerable band overlap, while we did not find Re^{3+} to support magnetism in these bilayers.

Moving to the d^5 column, 2LFeO leads to a simple spherical ion, high spin, antiferromagnet (AFM) ground state with no tendency to distort nor to assume topological nature. We find that $4d$ 2LRuO and $5d$ 2LOsO do not support a high spin state, due to weaker correlation effects than occur in Fe. The low spin state of 2LFeO can be obtained self-consistently for comparison, but it is 465 meV/Fe higher in energy and unlikely to be be synthesized. The resulting single hole in the low spin t_{2g} subshell reduces the orbital occupation complexity compared to the two-hole d^4 ions, but still shows important flexibility because the trigonal crystal field splitting of a_{1g} and e'_g is sensitive to the strain provided by the substrate.

For both Os and Ru, and for both lattice constants considered, restricting symmetry to $P321$ (*i.e.* symmetry equivalent X sites) and including SOC led to Chern insulating phases, as for the $3d$ cases X=Ti, Mn, and Co.[14] With the open d shell and being gapped by U, these are FM Chern Mott insulators. We restrict our discussion now to the relaxed, symmetry broken (inequivalent X sites) ground states,[12, 14] confirming the earlier results in the $3d$ series that full relaxation is essential to make realistic predictions. The basic ground state data are provided in Table I. Fig. 2 presents the band structures for 2LOsO and 2LRuO, first without (left panels) and then with SOC (right panels), for both values of the in-plane lattice constant.

A. $2LaOsO_3$

We first consider 2LOsO, whose largest SOC and smallest U and hence less tendency for large distortion, might seem to make it the more favorable candidate Chern insulator based on experience with the $3d$ series. The magnetism is robust, arising even at U=0. The $P1$ symmetry reflects two inequivalent Os sites, but the distortion in this case is minor. Without SOC, the bilayer @a_{LAO} (see Fig. 2) is a FM half metal with $1\mu_B$ spin moment per Os, while for @a_{LNO} the FM state is insulating and trivial. The impact of SOC is overwhelming – band mixing and shifting is so large that there is no visible correspondence between bands without and with SOC.

The orbital moments of the Os1 and Os2 ions are similar, $0.19\mu_B$ for a_{LAO} decreasing to $0.14\mu_B$ for a_{LNO}. Spin mixing by SOC reduces the total spin moment to $1.5\pm0.1\mu_B$. The gapless band structure for a_{LNO} becomes gapped to 46 meV for a_{LAO}, and the Chern number $\mathcal{C}$=2 establishes that the desired Chern insulating state has been found. As shown in Figs. 2, not only is 2LOsO metallic before SOC is included, but a narrow peak in the DOS at E_F (see the Supplemental Information) reflects a flat band region nearly coinciding with the Fermi level. For the $3d$ series, the SOC leaves bands mostly intact, only opening gaps at the Dirac point and quadratic band touching points, and opening anticrossings. In 2LOsO, SOC is very large and, as mentioned, bands before SOC cannot be lined up by eye with bands after SOC, *i.e.* entanglement is extensive. Thus for $5d$ ions, gaps are opened by widespread band rearrangements rather than by simple anticrossings. For 2LOsO, a very significant effect of the substrate lattice constant is that the distance between Os1 and Os2 layers, 2.52Å for a_{LAO}, reduces to 2.40Å for a_{LNO}.

B. $2LaRuO_3$

For 2LRuO at a_{LAO} without SOC, there is a tiny gap along $\Gamma - M$ near M, and an evident band inversion at M but apparently not at M' where there is a substantial gap. After SOC, the FM insulating state is preserved but trivial, so the apparent band inversion is not effective in producing a topological phase. The a_{LNO} case is the most interesting. The half metallic FM band structure becomes, upon including SOC, a $\mathcal{C} = -1$ Chern insulator with a 132 meV gap. Note, both from the data in Table I and the near symmetry of K and

K', and M and M', in the final bands in Fig. 2 that, as for 2LOsO, the Chern phase is very modestly distorted from $P321$ symmetry.

For 2LRuO, the distance d=2.42±0.01Å between Ru sites depends very little on the substrate lattice constant. At a_{LNO}, the Ru1-Ru2 inequivalence is small so the difference in orbital moments is minor, and the spin moment is hardly reduced by SOC. Before SOC is included a peak in the DOS (not shown) lying at E_F appears as for 2LOsO at a_{LAO}. The band giving rise to the peak is shifted by SOC (see below), resulting in a gap of 132 meV and a $\mathcal{C}$ = -1 Chern insulating phase. For 2LRuO at a_{LAO}, the two Ru sites show larger differences in orbital moments, 0.08 versus 0.16μ_B, see Table 1. SOC opens a large gap of 150 meV, but the state is found to be a trivial insulator. This last result suggests that the larger gap makes it impossible to sustain the band inversion and spin entanglement that is needed for the QAH phase.

The Berry curvatures $\Omega_z(\vec{k})$ of the two sister bilayers, pictured in Fig. 4, indicate very different distributions (as well as opposite signs). 2LOsO contains high and narrow peaks, distributed almost symmetrically around the K points along lines toward the three neighboring M points. The peaks lie near the minimum gap, a common occurrence. For 2LRuO, the seemingly minor breaking of three-fold symmetry becomes very obvious in Ω_z. The most intense peak arises near one M point, just off the $M-\Gamma$ line, and a secondary peak occurs in a similar position relative to the M' point. The fraction of area that contributes to $\mathcal{C} = -1$ is considerably larger in 2LRuO than that leading to $\mathcal{C}$=2 in 2LOsO.

III. DISCUSSION

Both 2LOsO and 2LRuO exhibit the sought-for Chern insulator (quantum anomalous Hall) state, with Chern numbers and gaps $\mathcal{C}$=2, 46 meV and $\mathcal{C}$=-1, 132 meV respectively, occurring for different choices of substrate. The magnitude of $\mathcal{C}$ suggests a guideline that larger values result from larger moments and strong SOC, as long as topological character can be maintained.[32] The strong dependence on lateral strain demonstrates that strain offers a means to manipulate Chern insulating phases as well as to engineer other properties, such as the Fermiology and superconductivity in Sr_2RuO_4 thin films.[33] Note that for both Os and Ru, larger orbital moments arise in the Chern phase than in the trivial state. Figure 3, emphasizing the bands of a_{1g} character (the rest of the character is e'_g) illustrates critical

effects of strain. Strain interchanges a_{1g} with e'_g character of the hole dramatically, and in both cases it is the one with strong a_{1g} hole character that promotes the Chern insulating phase. This result is consistent also with the observation that the Chern phases incur much less distortion than the trivial phases, because an a_{1g} hole is nondegenerate.

Some regularities can be observed in these results. Both 2LOsO@a_{LNO} and 2LRuO@a_{LAO} in Fig. 2, before accounting for SOC, show an uppermost occupied band lying at E_F that is flat over much of the zone. These are the cases with smaller orbital moments and they have larger gaps once SOC in included, and they are also the trivial insulating states. The other two cases – the Chern phases – are mildly symmetry broken from threefold symmetry. The Dirac point at K in the unoccupied bands of 2LRuO is hardly gapped at all, and the orbital moments of the two sites are identical. In this way they resemble their $3d$ counterparts X=Ti, Mn, Co for imposed threefold symmetry. The spectrum is topological, but when symmetry is broken more strongly, entanglement is lost. This result is what our "pre-design" (on the series of $3d$ ions) had led us to conclude.[14] A significant new result is that the topological nature can be tuned with even a modest amount of strain.

Our main result is that the Ru buckled honeycomb layer provides a QAH (Chern) insulator with a gap of 132 meV. Secondarily, the isovalent Os bilayer provides a Chern insulating state with a gap of 46 meV. The calculated anomalous Hall conductivities correspond to Chern numbers $\mathcal{C}$=-1 and $\mathcal{C}$ = +2, respectively.

As mentioned in the Introduction, strong interaction U, large SOC ξ, and strain are coupled in their impact. A schematic phase diagram is presented in Fig. 5 in (strain,U,ξ) space. Isovalent Ru and Os lie along a line of probable Chern phases, as pictured. However, since the Chern number changes between the established points, either (1) the gap must close and then re-open with a different Chern number, or (2) a first-order phase transition must occur, which cannot be foreseen without an accurate theory of the free energy. Ru-Os alloy bilayers thus provide a rich region for further study. Fortunately, high quality (111) film growth of this kind has been reported for iridates,[18, 22] making synthesis and applications with Os and Ru quite promising. We hope that these results will stimulate intense experimental study of these materials.

IV. METHODS

First-principles DFT-based electronic structure calculations were performed using the full-potential linearized augmented plane wave method as implemented in the WIEN2k code [34]. For the exchange-correlation functional we used the generalized gradient approximation (GGA)[35]. Static local electronic correlations were added to the GGA exchange correlation potential in the GGA+U method [36] with U_{Os}=1 eV, U_{Ru}=3 eV (for the $3d$ analog, $U_{Fe} \sim$ 5 eV). $U = 8$ eV on the La $4f$ orbitals is applied to displace them upward somewhat. The results were found to be robust with respect to reasonable variations of the onsite Coulomb repulsion parameter.

The influence of strain was investigated by setting the lateral lattice constant to $a_{LAO} = 3.79\mathring{A}$ or $a_{LNO} = 3.86\mathring{A}$, which correspond to superlattices grown either on an LAO(111) substrate, or an LNO substrate with 1.8% tensile strain. The out-of-plane lattice parameter c was first chosen to be consistent with that of $(LaNiO_3)_2/(LaAlO_3)_4(111)$ studied by Doennig and co-authors[13], then we performed lattice parameter optimizations to obtain the optimized value of c and the internal coordinates. Octahedral tilts and distortions were allowed when relaxing atomic positions, consistent with the overall symmetry. Calculations were first done with symmetry constrained to space group $P321$ (threefold rotation plus inversion), then unconstrained to $P1$ symmetry (no symmetry) to obtain full relaxation.

A $20 \times 20 \times 6$ k-point mesh was used for self-consistency. Structural relaxations were carried out with SOC included. SOC was also included in the electronic properties calculations with a (001) spin direction. Subsequently we used Wannier interpolation based on maximally localized Wannier functions (MLWFs) to calculate the Berry curvature and the anomalous Hall conductivity to obtain the Chern number. The final zone integration requires a very dense k-point grid in the BZ [37–39]

The Bloch wave functions were projected onto the d local orbitals of Os and Ru to obtain MLWFs,[37] which serve as the basis for further analysis. The MLWF-interpolated energy bands are in excellent agreement with the Wien2k bands. The Berry curvature $\Omega_z(\boldsymbol{k})$ is obtained from all bands below the Fermi level beginning from the definition

$$\Omega_z(\boldsymbol{k}) = -\sum_{n}^{occ}\sum_{m}^{unocc} 2Im\frac{\langle u_{n\boldsymbol{k}}|v_x|u_{m\boldsymbol{k}}\rangle\langle u_{m\boldsymbol{k}}|v_y|u_{n\boldsymbol{k}}\rangle}{(\varepsilon_{m\boldsymbol{k}} - \varepsilon_{n\boldsymbol{k}})^2} \tag{1}$$

and performing manipulations required by the use of a finite set of MLWFs.[38] The Berry

curvature is integrated over the Brillouin zone to obtain the anomalous Hall conductivity (AHC) using

$$\sigma_{xy} = -\frac{e^2}{\hbar}\sum_n \int_{BZ} \frac{d\boldsymbol{k}}{(2\pi)^3} f_n(\boldsymbol{k})\Omega_{n,z}(\boldsymbol{k}) = -\frac{e^2}{\hbar}C, \tag{2}$$

where $\sigma_{xy} = -\sigma_{yx}$ is the antisymmetric part of the conductivity. The Chern numbers were computed by sampling a dense k-point grid of $300 \times 300 \times 50$.

V. ACKNOWLEDGMENTS.

The authors acknowledge useful discussions with D. Arovas, A. Essin, K. Koepernik, K.-L. Lee, V. Pardo, and Y. Quan.

VI. CONTRIBUTIONS

This project was conceived by W.E.P. and R.P., and supervised by W.E.P. Calculations were carried out on the Ru and Os systems by H.G., with important assistance provided by S.G. O.K. performed the calculations on the Fe systems. All authors contributed to the analysis.

VII. COMPETING INTERESTS

The authors declare no competing interests.

VIII. FUNDING

The calculations were performed in Environmental Molecular Sciences Laboratory at the PNNL and National Energy Research Scientific Computing Centre (NERSC). This work was supported by the China Scholarship Council and the NSFC 21373190 (H.G.), by US Department of Energy grant DE-FG03-03NA00071 (S.G.), by the German Science Foundation within SFB/TR80, project G3 (R.P.), and by US National Science Foundation Grant DMR-1534719 (W.E.P.) under the Designing Materials to Engineer and Revolutionize our

Future program.

---

[1] D. J. Thouless, M. Kohmoto, M. P. Nightingale, and M. den Nijs, Quantized Hall Conductance in a Two-Dimensional Periodic Potential, Phys. Rev. Lett. **49**, 405 (1982).

[2] F. D. M. Haldane, Model for a Quantum Hall Effect without Landau Levels: Condensed-Matter Realization of the "Parity Anomaly," Phys. Rev. Lett. **61**, 2015 (1988).

[3] A. H. Castro Neto, F. Guinea, N. M. R. Peres, K. S. Novoselov, and A. K. Geim, The electronic properties of graphene, Rev. Mod. Phys. **81**, 109 (2009).

[4] D. Xiao, W. Zhu, Y. Ran, N. Nagaosa, and S. Okamoto, Interface engineering of quantum Hall effects in digital transition metal oxide heterostructures, Nat. Commun. **2**, 596 (2011).

[5] A. R. Wright, Realising Haldane's vision for a Chern insulator in buckled lattices, Sci. Rep. **3**, 2736 (2013).

[6] A. Rüegg and G. A. Fiete, Topological insulators from complex orbital order in transition-metal oxides heterostructures, Phys. Rev. B **84**, 201103 (2011).

[7] K.-Y. Yang, W. Zhu, D. Xiao, S. Okamoto, Z. Wang, and Y. Ran, Phys. Possible interaction-driven topological phases in (111) bilayers of $LaNiO_3$, Rev. B **84**, 201104(R) (2011).

[8] A. Rüegg, C. Mitra, A. A. Demkov, and G. A. Fiete, Electronic structure of $(LaNiO_3)_2/(LaAlO_3)_N$ heterostructures grown along [111], Phys. Rev. B **85**, 245131 (2012).

[9] S. Okamoto, Doped Mott Insulators in (111) Bilayers of Perovskite Transition-Metal Oxides with a Strong Spin-Orbit Coupling, Phys. Rev. Lett. **110**, 066403 (2013).

[10] J. Lado, V. Pardo, and D. Baldomir, *Ab initio* study of Z_2 topological phases in perovskite (111) $(SrTiO_3)_7(SrIrO_3)_2$ and $(KTaO_3)_7(KPtO_3)_2$ multilayers, Phys. Rev. B **88**, 155119 (2013).

[11] S. Okamoto, W. Zhu, Y. Nomura, R. Arita, D. Xiao, and N. Nagaosa, Correlation effects in (111) bilayers of perovskite transition-metal oxides. Phys. Rev. B **89**, 195121 (2014).

[12] D. Doennig, W. E. Pickett, and R. Pentcheva, Massive Symmetry Breaking in $LaAlO_3/SrTiO_3$(111) Quantum Wells: A Three-Orbital, Strongly Correlated Generalization of Graphene, Phys. Rev. Lett. **111**, 126804 (2013).

[13] D. Doennig, W. E. Pickett, and R. Pentcheva, Confinement-driven Transitions between Topological and Mott Phases in (LaNiO3)N/(LaAlO3)M(111) Superlattices Phys. Rev. B **89**,

121110 (2014).

[14] D. Doennig, S. Baidya, W. E. Pickett, and R. Pentcheva, Design of Chern and Mott insulators in buckled 3*d* oxide honeycomb lattices, Phys. Rev. B **93**, 165145 (2016).

[15] Y. Weng, X. Huang, Y. Yao, and S. Dong, Topological magnetic phase in $LaMnO_3$ (111) bilayer, Phys. Rev. B **92**, 195114 (2015).

[16] Y. Wang, Z. Wang, Z. Fang, and X. Dai, Interaction-induced quantum anomalous Hall phase in (111) bilayer of $LaCoO_3$, Phys. Rev. B **91**, 125139 (2015).

[17] Y. Chen and H.-Y. Kee, Topological phases in iridium oxide superlattices: quantized anomalous charge or valley Hall insulators, Phys. Rev. B **90**, 195145 (2014).

[18] D. Hirai, J. Matsuno, and H. Takagi, Fabrication of (111)-oriented $Ca_{0.5}Sr_{0.5}IrO_3/SrTiO_3$ superlattices – a designed playground for honeycomb physics, APL Matl. **3**, 041508 (2015).

[19] J. Matsuno *et al.*, Engineering a spin-orbital magnetic insulator by tailoring superlattices, Phys. Rev. Lett. **114**, 247209 (2015).

[20] Y. Jia *et al.*, Exchange coupling in (111)-oriented $La_{0.7}Sr^{0.3}MnO_3/La_{0.7}Sr^{0.3}FeO_3$ superlattices, Phys. Rev. B **92**, 094407 (2015).

[21] Y. F. Nie *et al.*, Interplay of spin-orbit interaction, dimensionality, and octahedral rotations in semimetallic $SrIrO_3$, Phys. Rev. Lett. **114**, 016401 (2015).

[22] T.J. Anderson *et al.*, Metastable honeycomb $SrTiO_3/SrIrO_3$ heterostructures, Appl. Phys. Lett. **108**, 151604 (2016).

[23] Y. Jia *et al.*, Thickness dependence of exchange coupling in (111)-oriented perovskite oxide superlattices, Phys. Rev. B **93**, 104403 (2016).

[24] T. H. Kim *et al.*, Polar metals by geometric design, Nature **533**, 68 (2016).

[25] S. Middey, S. Debnath, P. Mahadevan, and D. D. Sarma, $NaOsO_3$: A high Neel temperature 5*d* oxide, Phys. Rev. B **89**, 134416 (2014).

[26] H. Huang, Z. Liu, H. Zhang, W. Duan, and D. Vanderbilt, Emergence of a Chern-insulating state from a semi- Dirac dispersion, Phys. Rev. B **92**, 161115(R) (2015)

[27] V. Pardo and W. E. Pickett, Half-metallic semiDirac Point Generated by Quantum Confinement in TiO_2/VO_2 Nanostructures, Phys. Rev. Lett. **102**, 166803 (2009).

[28] T. Cai, X. Li, F. Wang, S. Ju, J. Feng, and C.-D. Gong, Single-spin Dirac Fermion and Chern insulator based on simple oxides, Nano Lett. **15**, 6434 (2015).

[29] V. Pardo and W. E. Pickett, Compensated magnetism by design in double perovskite oxides, Phys. Rev. B **80**, 054415 (2009).

[30] H. J. Xiang and M.-H. Whangbo, Cooperative effect of electron correlation and spin-orbit coupling on the electronic and magnetic properties of Ba_2NaOsO_6, Phys. Rev. B **75**, 052407 (2007).

[31] S. Gangopadhyay and W. E. Pickett, Spin-orbit coupling, strong correlation, and insulator-metal transitions: The $J_{eff} = 3/2$ ferromagnetic Dirac-Mott insulator Ba_2NaOsO_6, Phys. Rev. B **91**, 045133 (2015).

[32] J. Wang, B. Lian, H. Zhang, Y. Xu, and S.-C. Zhang, Quantum anomalous Hall effect with higher plateaus, Phys. Rev. Lett. **111**, 136801 (2013).

[33] B. Burganov *et al.*, J.W. Harter, D.E. Shai, A.S. Gibbs, A.P. Mackenzie, R. Uecker, M. Bruetzam, M.R. Beasley, C.J. Fennie, D.G. Schlom, and K.M. Shen, Strain Control of Fermiology and Many-Body Interactions in Two-Dimensional Ruthenates, Phys. Rev. Lett. **116**, 197003 (2016).

[34] P. Blaha, K. Schwarz, G. K. H. Madsen, D. Kvasnicka, and J. Luitz, *WIEN2k, An Augmented Plane Wave Plus Local Orbitals Program for Calculating Crystal Properties*, ISBN 3-9501031-1-2 (Vienna University of Technology, Vienna, Austria, 2001).

[35] J. P. Perdew, K. Burke and M. Ernzerhof, Generalized Gradient Approximation Made Simple, Phys. Rev. Lett. **77**, 3865 (1996).

[36] E. R. Ylvisaker, K. Koepernik, and W. E. Pickett, Anisotropy and Magnetism in the LSDA+U Method, Phys. Rev. B **79**, 035103 (2009).

[37] A. A. Mostofi, J. R. Yates, Y. S. Lee, I. Souza, I. Vanderbilt, N. Marzari, *wannier90*: A tool for obtaining maximally-localised Wannier functions, Comput. Phys. Commun. **178**, 685 (2008).

[38] X. Wang, J. R. Yates, I. Souza, D. Vanderbilt, *Ab initio* calculation of the anomalous Hall conductivity by Wannier interpolation, Phys. Rev. B **74**, 195118 (2006).

[39] J. Kuneš, R. Arita, P. Wissgott, A. Toschi, H. Ikeda, K. Held, Wien2wannier: From linearized augmented plane waves to maximally localized Wannier functions, Comp. Phys. Commun. **181**, 1888 (2010).

Table Caption

Table 1. Characteristics of the ground states of the d^5 buckled honeycomb systems 2LRuO and 2LOsO, fully relaxed ($P1$ symmetry) and including spin-orbit coupling, for each of the two lattice constants. $\Delta z_{M,M} = d_{M,M'}$ is the separation of the two metal (Ru or Os) layers, equal to $a/\sqrt{3}$ for an unrelaxed structure with lattice constant a. m_{orb} is the orbital moment of each of the inequivalent metal ions. m_{sp} is the spin moment per ion (half the total).

Figure Captions

Figure 1. Geometry of this honeycomb lattice system. (a) Side view of one cell of the $(LAO)_4/(LXO)_2(111)$ superlattice. (b) Top view of the 2LXO bilayer forming a buckled honeycomb lattice (lower right) from bilayer of Os cations. Blue sites lie in a plane above the plane containing the pink sites.

Figure 2. Top four panels: band structures of the fully relaxed buckled bilayers corresponding to lattice constant a_{LAO}, for both 2LOsO and 2LRuO. Majority and minority bands are plotted in blue and yellow, respectively. Left panels, before including SOC; right panels, with SOC included. Lower four panels, analogous plots for a_{LNO}. Note that SOC converts the half metallic FM spectrum for 2LOsO to the gapped Chern insulator $\mathcal{C}$=2 phase.

Figure 3. Fat band plot highlighting the a_{1g} character at the a_{LAO} lattice constant. The remaining character is primarily e'_g. The Chern phases have large a_{1g} hole character, which as these results demonstrate is sensitive to strain.

Figure 4. Surface plot (left) and 2D projected colorplot of the Berry curvatures $\Omega_z(\vec{k})$ of (upper) 2LOsO ($\mathcal{C} = 2$) and (lower) 2LRuO ($\mathcal{C} = -1$). The character of Ω_z is very different for the two Chern insulating states.

Figure 5. Schematic diagram in the substrate strain – repulsion U – spin-orbit coupling strength ξ space of the region explored in this work. The area, linear in U, is provided for perspective. The long-dashed diagonal line connects the two Chern phases, as discussed in the text.

TABLE I. Characteristics of the ground states of the d^5 buckled honeycomb systems 2LRuO and 2LOsO, fully relaxed ($P1$ symmetry) and including spin-orbit coupling, for each of the two lattice constants. $\Delta z_{M,M} = d_{M,M'}$ is the separation of the two metal (Ru or Os) layers, equal to $a/\sqrt{3}$ for an unrelaxed structure with lattice constant a. m_{orb} is the orbital moment of each of the inequivalent metal ions. m_{sp} is the spin moment per ion (half the total).

2LRuO	a_{LAO}	a_{LNO}
Gap (meV)	*150*	**132**
Chern number	*0*	**-1**
$d_{M,M}$ (Å)	2.43	2.41
$m_{orb}(\mu_B)$	0.08,0.16	0.16,0.16
m_{sp}	0.99	0.99
2LOsO	a_{LAO}	a_{LNO}
Gap (meV)	**46**	*115*
Chern number	**2**	*0*
$d_{M,M}$ (Å)	2.52	2.40
$m_{orb}(\mu_B)$	0.19,0.19	0.14,0.13
m_{sp}	0.81	0.71

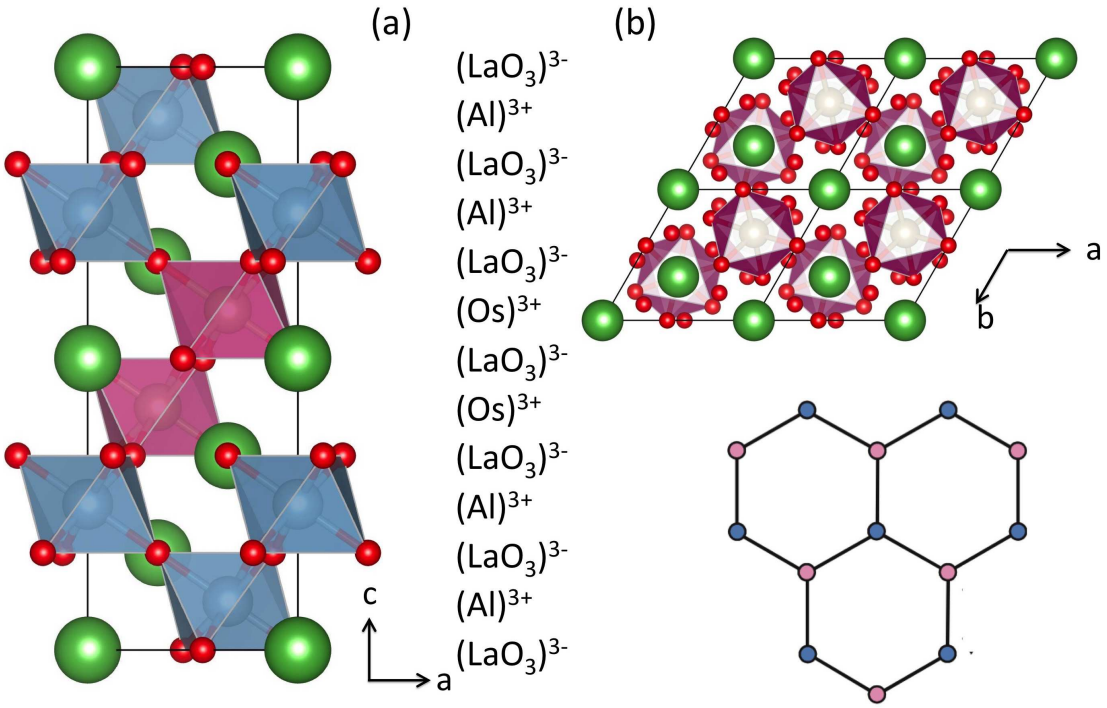

FIG. 1. Geometry of this honeycomb lattice system. (a) Side view of one cell of the $(LAO)_4/(LXO)_2(111)$ superlattice. (b) Top view of the 2LXO bilayer forming a buckled honeycomb lattice (lower right) from bilayer of Os cations. Blue sites lie in a plane above the plane containing the pink sites.

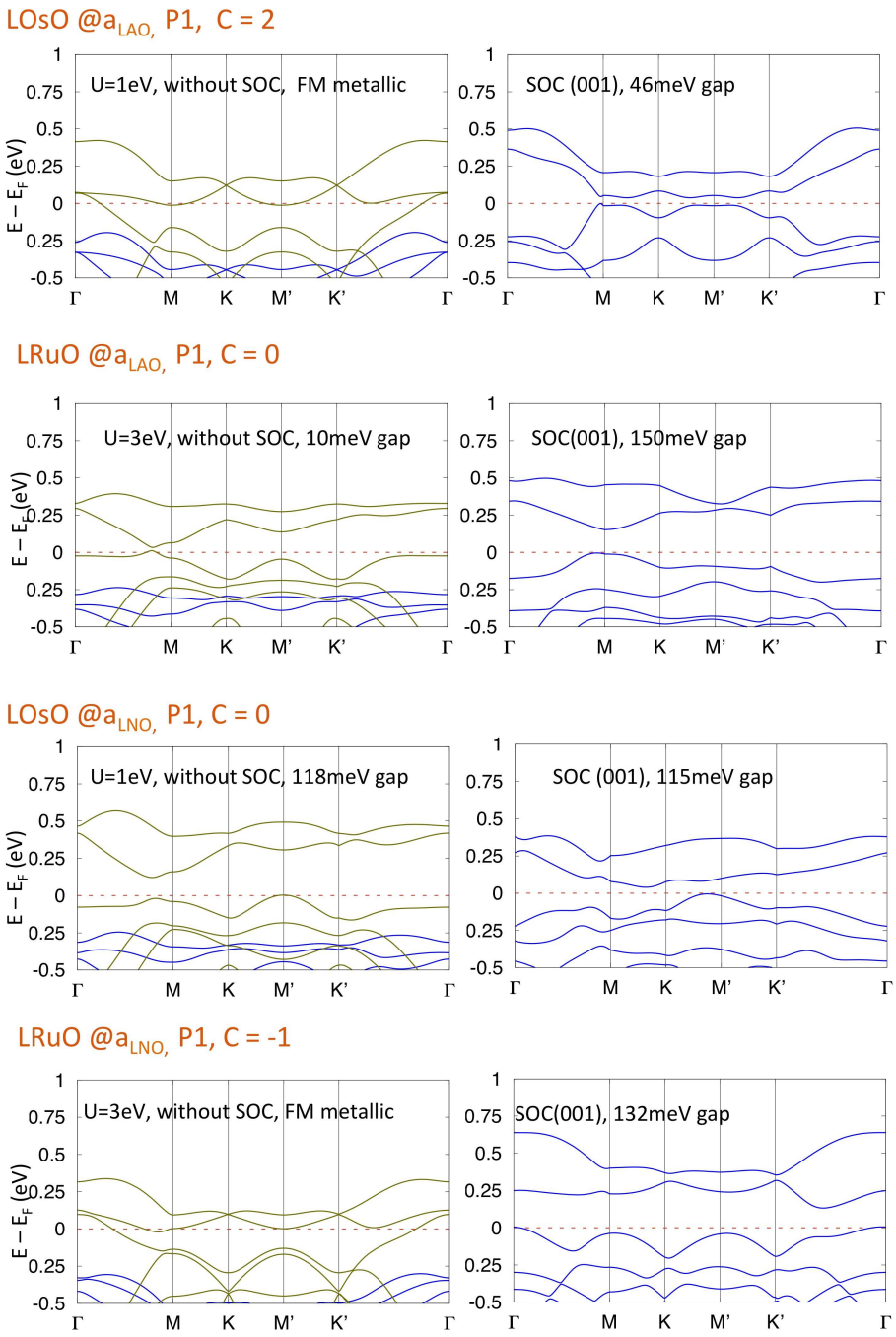

FIG. 2. Top four panels: band structures of the fully relaxed buckled bilayers corresponding to lattice constant a_{LAO}, for both 2LOsO and 2LRuO. Majority and minority bands are plotted in blue and yellow, respectively. Left panels, before including SOC; right panels, with SOC included. Lower four panels, analogous plots for a_{LNO}. Note that SOC converts the half metallic FM spectrum for 2LOsO to the gapped Chern insulator $\mathcal{C}$=2 phase.

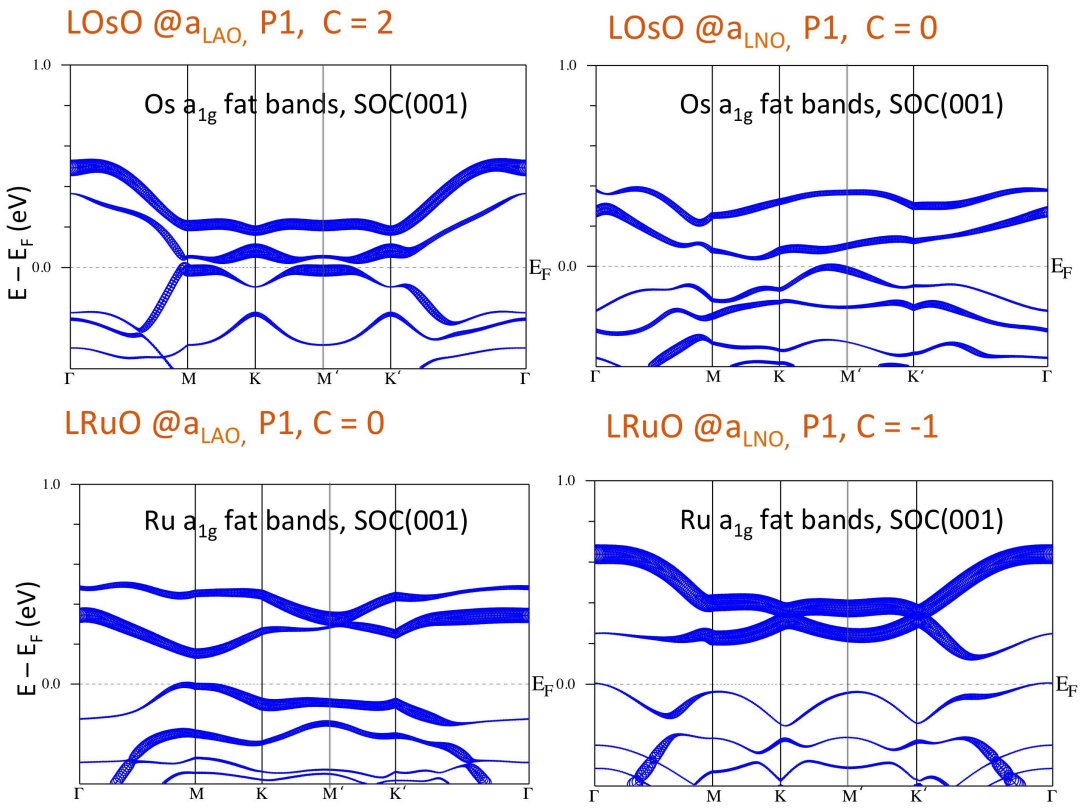

FIG. 3. Fat band plot highlighting the a_{1g} character at the a_{LAO} lattice constant. The remaining character is primarily e'_g. The Chern phases have large a_{1g} hole character, which as these results demonstrate is sensitive to strain.

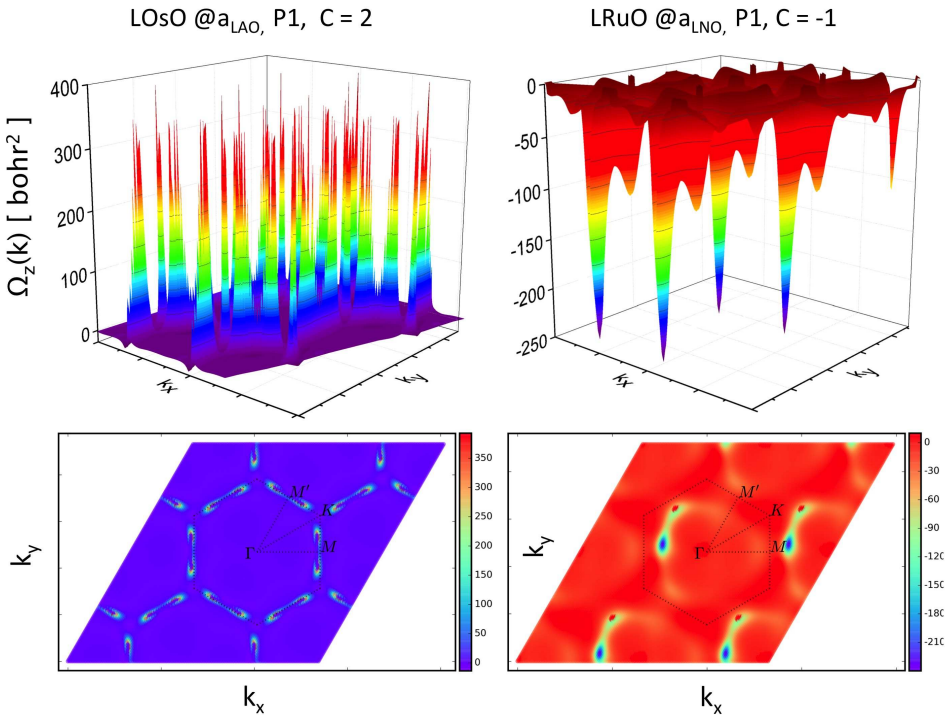

FIG. 4. Surface plot (left) and 2D projected colorplot of the Berry curvatures $\Omega_z(\vec{k})$ of (upper) 2LOsO ($\mathcal{C} = 2$) and (lower) 2LRuO ($\mathcal{C} = -1$). The character of Ω_z is very different for the two Chern insulating states.

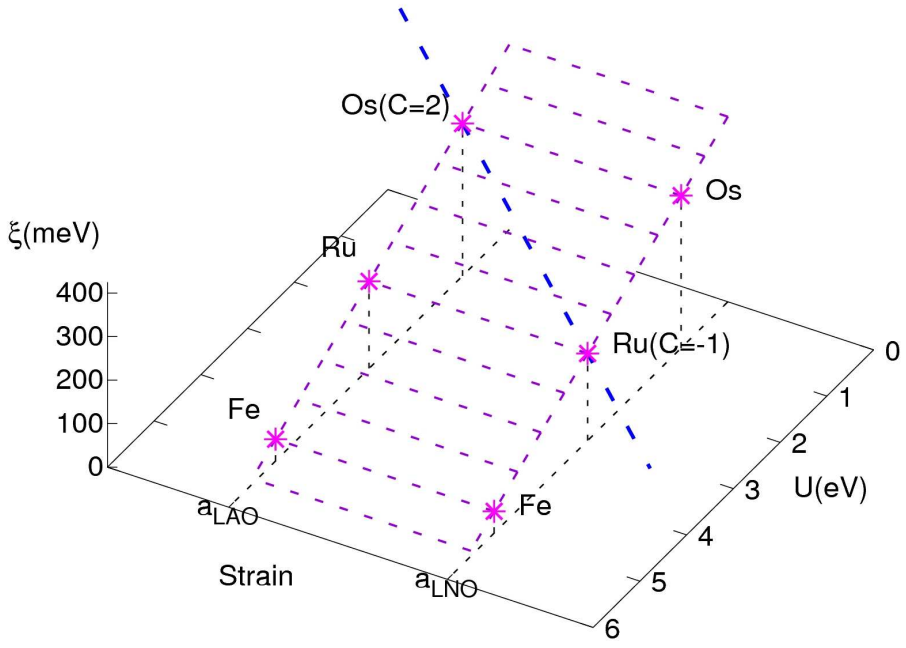

FIG. 5. Schematic diagram in the substrate strain – repulsion U – spin-orbit coupling strength ξ space of the region explored in this work. The area, linear in U, is provided for perspective. The long-dashed diagonal line connects the two Chern phases, as discussed in the text.